Synthesis of liquid fuel via direct hydrogenation of CO_2

Zhenhong He[a,b], Meng Cui[a,c], Qingli Qian[a,d,1], Jingjing Zhang[a,c], Huizhen Liu[a,c,d], and Buxing Han[a,c,d,1]

[a]Beijing National Laboratory for Molecular Sciences, CAS Key Laboratory of Colloid, Interface and Chemical Thermodynamics, CAS Research/Education Center for Excellence in Molecular Sciences, Institute of Chemistry, Chinese Academy of Sciences, Beijing 100190, China; [b]College of Chemistry and Chemical Engineering, Shaanxi University of Science & Technology, Xi'an, Shaanxi, 710021, China; [c]School of Chemistry and Chemical Engineering, University of Chinese Academy of Sciences, Beijing 100049, China; and [d]Physical Science Laboratory, Huairou National Comprehensive Science Center, Beijing 101400, China

Edited by Richard Eisenberg, University of Rochester, Rochester, NY, and approved May 14, 2019 (received for review December 13, 2018)

Synthesis of liquid fuels (C_{5+} hydrocarbons) via CO_2 hydrogenation is very promising. Hydrogenation of CO_2 to liquid hydrocarbons usually proceeds through tandem catalysis of reverse water gas shift (RWGS) reaction to produce CO, and subsequent CO hydrogenation to hydrocarbons via Fischer–Tropsch synthesis (FTS). CO_2 is a thermodynamically stable and chemically inert molecule, and RWGS reaction is endothermic and needs a higher temperature, whereas FTS reaction is exothermic and is thermodynamically favored at a lower temperature. Therefore, the reported technologies have some obvious drawbacks, such as high temperature, low selectivity, and use of complex catalysts. Herein we discovered that a simple Co_6/MnO_x nanocatalyst could efficiently catalyze CO_2 hydrogenation. The reaction proceeded at 200 °C, which is much lower than those reported so far. The selectivity of liquid hydrocarbon (C_5 to C_{26}, mostly *n*-paraffin) in total product could reach 53.2 C-mol%, which is among the highest reported to date. Interestingly, CO was hardly detectable during the reaction. The in situ Fourier transform infrared characterization and ^{13}CO labeling test confirmed that the reaction was not via CO, accounting for the eminent catalytic results. This report represents significant progress in CO_2 chemistry and CO_2 transformation.

CO_2 hydrogenation | liquid fuel | paraffin | lower temperature | reaction pathway

Transformation of CO_2 into value-added chemicals has attracted much attention in past decades (1–5). Liquid hydrocarbons (more than five carbon atoms, i.e., C_{5+}) are widely used as liquid fuels, which are currently produced from fossil resources, especially petroleum. The growing demand for liquid fuels and gradual depletion of petroleum lead to the urgent need for their production from renewable resources. Hydrogen gas is a clean reductant, which can be produced from water by artificial photosynthesis or by electricity from renewable energy such as wind and solar energy, and this area is developing rapidly (6, 7). Moreover, CO_2 hydrogenation into liquid hydrocarbons is an interesting topic in chemistry (8–15). However, at the present stage, it is still a great challenge. Firstly, CO_2 is a fully oxidized, thermodynamically stable and chemically inert molecule. Secondly, the difficulty of CO_2 adsorption on a catalyst surface may result in a low C/H ratio at catalytic sites, favoring methane formation and inhibiting the chain growth probability (8, 9). To date, most reports of CO_2 hydrogenation have been focusing on C_1 or short-chain products, such as CO, HCOOH, CH_3OH, CH_4, and C_2 to C_4 olefins, while studies on producing liquid (C_{5+}) hydrocarbons are rarely reported (8–11).

Hydrogenation of CO_2 to liquid hydrocarbons usually proceeds through tandem catalysis of reverse water gas shift (RWGS) reaction and subsequent CO hydrogenation to hydrocarbons via Fischer–Tropsch synthesis (FTS) (8, 9). The RWGS reaction is endothermic and needs a higher temperature, whereas the FTS reaction is exothermic and favors a lower temperature. Hence this reaction path has inherent drawbacks. Firstly, complicated catalysts are usually required to tailor the cascade reactions, and a high temperature (usually above 300 °C) is often needed to drive these reactions. Secondly, the equilibrium of the RWGS reaction limits the pressure of CO generated in situ, which restricts the selectivity of liquid hydrocarbon in subsequent FTS reaction. Hence, an additional reforming catalyst is usually required to obtain good catalytic results. Thirdly, considerable CO is inevitably retained in the final product, which usually occupies about 20 to 45% of the total product. Although, in several cases, methanol acted as an intermediate to produce liquid hydrocarbon from CO_2 hydrogenation at high temperature, considerable CO byproduct also existed in the final product. Iron-based catalysts, which could catalyze both RWGS and FTS reactions, were predominantly used as a catalyst for CO_2 hydrogenation to longer-chain hydrocarbons, especially olefins (16, 17). Very recently, significant progress has been made in hydrogenating CO_2 into gasoline fuel. It was found that, in a flow reactor, Na–Fe_3O_4/HZSM-5 multifunctional catalyst (14) and In_2O_3/HZSM-5 bifunctional catalyst (15) showed excellent performance in converting CO_2 and H_2 into liquid fuel at about 320 °C. In the reaction, CO was an intermediate and/or considerable byproduct. Obviously, a novel catalyst for liquid fuel synthesis via CO_2 hydrogenation that can avoid CO is highly desirable.

In a previous paper, we developed a route to synthesize acetic acid via methanol hydrocarboxylation over a homogeneous catalyst, where CO was almost undetectable and CO_2 directly participated in forming carboxyl of the acetic acid (5). Here we report the high-selective synthesis of liquid hydrocarbons via CO_2 hydrogenation at a lower temperature using a simple Co_6/MnO_x nanocatalyst. Interestingly, very little CO was detected in the product. Further study indicates that hydrogenation of CO_2 to form C_{5+} paraffins did not proceed through the CO pathway.

Results and Discussion

Catalyst Structure. The Co_6/MnO_x nanocatalyst was prepared by a coprecipitation method. The transmission electron microscope

Significance

CO_2 is a greenhouse gas. Synthesis of liquid fuel using CO_2 and H_2 is promising for the sustainability of mankind. The reported technologies usually proceed via CO intermediate, which needs high temperature, and tend to cause low selectivity. Direct hydrogenation of CO_2 to liquid fuel, not via CO, is a challenging issue. In this work, we designed a Co_6/MnO_x nanocatalyst that could successfully avoid the CO route. The reaction could proceed at 200 °C, which is much lower than those reported so far. The selectivity of the liquid fuel in total products reached 53.2 C-mol%, which is among the highest reported to date.

Author contributions: Z.H., Q.Q., and B.H. designed research; Z.H., M.C., Q.Q., J.Z., and B.H. performed research; M.C., J.Z., and H.L. analyzed data; and Z.H., Q.Q., and B.H. wrote the paper.

The authors declare no conflict of interest.

This article is a PNAS Direct Submission.

[1]To whom correspondence may be addressed. Email: qianql@iccas.ac.cn or hanbx@iccas.ac.cn.

This article contains supporting information online at www.pnas.org/lookup/suppl/doi:10.1073/pnas.1821231116/-/DCSupplemental.

Published online June 10, 2019.

(TEM) image shows that the size of the catalyst particles was mostly in the range of 25 nm to 40 nm (Fig. 1*A*). The N_2 adsorption test revealed that the Brunauer–Emmett–Teller surface area of the piled catalyst was only 49.4 m^2/g (*SI Appendix*, Fig. S1), indicating that it was not a porous material. The metallic Co (Co^0) catalyst and the Co–Mn bimetallic catalysts fabricated by the above method were all spherical-like, and the sizes of the bimetallic catalysts were slightly larger (*SI Appendix*, Fig. S2). In the TEM images of Co_6/MnO_x, the lattice spacings of 1.92 and 2.02 Å (Fig. 1*B*) corresponded to the (101) plane and the (002) plane of Co^0, and the lattice spacing of 2.57 Å (Fig. 1*C*) could be assigned to the (111) plane of MnO. The X-ray diffraction (XRD) pattern also reveals two kinds of crystal phases, i.e., Co^0 bulk phase and MnO, in the catalyst (*SI Appendix*, Fig. S3). It is known that cobalt oxides can be easily reduced to metallic Co by H_2 (18). The temperature-programmed reduction (TPR) analysis proved that the Mn atoms could evidently retard the reduction of Co oxides because strong interaction existed between Co–Mn atoms (*SI Appendix*, Fig. S4). The X-ray photoelectron spectroscopy (XPS) characterization suggests that Co^{2+} and Mn^{3+} were on the surface of the catalyst (*SI Appendix*, Fig. S5 *A–C*). The elementary mapping shows that Co, Mn, and O atoms were well dispersed in the catalyst (*SI Appendix*, Fig. S6). The inductively coupled plasma optical emission spectroscopy (ICP-OES) and XPS analysis demonstrated that compositions of the catalysts and catalyst surface were consistent with the design values (*SI Appendix*, Table S1). In brief, the Co_6/MnO_x consisted of Co^0 and MnO crystallites, and strong interaction existed between the atoms.

Catalytic Performance. The target reaction was effectively catalyzed by Co_6/MnO_x in squalane solvent at milder conditions (Table 1). Liquid hydrocarbons (C_5 to C_{26}) were the major product, and their selectivity in the total product was as high as 53.2 C-mol% (Table 1, entry 1). The alkane products were all linear alkanes (*n*-paraffins). The byproducts were mostly C_1 to C_4 hydrocarbons. The C atoms in the hydrocarbons were all from CO_2, because no product was observed without the reactant CO_2 (entry 2). The reaction temperature was 200 °C, which is much lower than those reported in the literature using a flow reactor. The detailed product distribution (*SI Appendix*, Fig. S7 *A* and *B*) indicated that a high proportion of *n*-paraffins, especially C_{5+} *n*-paraffins, was obtained in the reaction. The chain length distribution of the hydrocarbon products followed the Anderson–Schulz–Flory (ASF) statistics (*SI Appendix*, Fig. S7*C*). The chain growth probability (α) was 0.78, which is consistent with a large portion of longer-chain products. Interestingly, the amount of CO was very small (0.4 C-mol%). Further studies also showed that CO was hardly detectable during the whole reaction, which will be discussed in the following paragraphs. We would like to mention that the above results were collected using a batch reactor, where CO_2 and H_2 reacted on suspending catalyst particles under stirring. The product generated remained in the reactor during the reaction. While in a flow reactor, reactant gases of constant pressure passed through the packed catalyst bed, and the products generated were simultaneously taken out of the reactor by flowing gas.

To optimize the catalyst, we tested the Co^0 and its oxides (CoO, Co_3O_4) in CO_2 hydrogenation. The results revealed that Co^0 could catalyze the synthesis of C_{5+} hydrocarbons at very low activity and C_{5+} selectivity, and the largest compound contained only 16 C atoms (Table 1, entry 3), whereas the Co oxides could not catalyze the reaction at all (entries 4, 5). We also used the metallic Mn and its oxides (MnO, MnO_2), but the reaction did not occur either (entries 6 to 8). Thus, we deduce that Co was the

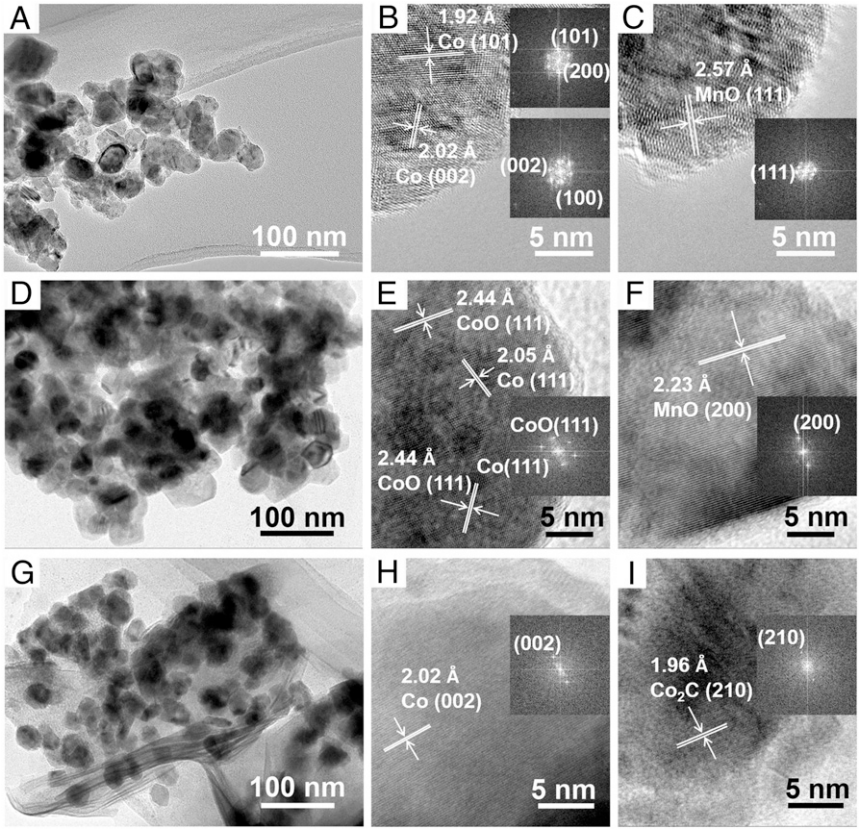

Fig. 1. TEM images of Co_6/MnO_x and fast Fourier transform patterns (*Insets*): the fresh catalyst (*A–C*); the catalyst after CO_2 hydrogenation (*D–F*), and the catalyst after CO hydrogenation (*G–I*).

Table 1. CO_2 hydrogenation using different catalysts

Entry	Catalyst	Solvent	Selectivity (C-mol%) CO	C_{1-4}	C_{5+}	ROH	Activity ($mmol_{CO2}·g_{cat}^{-1}·h^{-1}$)
1*	Co_6/MnO_x	squalane	0.4	46.4	53.2	0	15.1
2†	Co_6/MnO_x	squalane	—	—	—	—	0
3	Co^0	squalane	0.6	80.7	18.7	0	1.7
4	CoO	squalane	0	0	0	0	0
5	Co_3O_4	squalane	0	0	0	0	0
6	Mn	squalane	0	0	0	0	0
7	MnO	squalane	0	0	0	0	0
8	MnO_2	squalane	0	0	0	0	0
9	Co_{14}/MnO_x	squalane	0.5	58.5	41.0	0	6.6
10	Co_{10}/MnO_x	squalane	0.5	47.2	52.3	0	11.2
11	Co_2/MnO_x	squalane	0.4	76.2	23.4	0	13.3
12	Co_6/ZnO_x	squalane	0.1	80.7	19.2	0	4.8
13	Co_6/AlO_x	squalane	0.1	94.2	5.7	0	4.1
14	Co_6/CeO_x	squalane	0.4	89.8	9.8	0	6.3
15	Co_6/MnO_x	—	0.7	60.9	38.4	0	11.3
16	Co_6/MnO_x	cyclohexane	0.4	48.3	51.3	0	14.7
17	Co_6/MnO_x	benzene	0.5	95.3	4.2	0	7.9
18	Co_6/MnO_x	DMI	0.6	87.6	6.8	5.0	2.6
19	Co_6/MnO_x	water	0.3	92.9	0	6.8	3.2

Reaction conditions: 20 mg of catalyst, 1.0 mL of solvent (squalane), 200 °C, 15 h, initial pressure 8 MPa (CO_2/H_2 = 1).

*The conversion of CO_2 was 15.3%, and the selectivity of paraffin in the total hydrocarbons was 78.1 C-mol%; moreover, the selectivity of paraffin in the C_{5+} products was 67.2 C-mol%.

†No CO_2 was added. The error of activity was ±1.0 $mmol_{CO2}·g_{cat}^{-1}·h^{-1}$ and the error of selectivity was ±1.5 C-mol%, which were obtained by three repeated experiments.

major catalyst, and Mn was the promoter. After testing the Co-Mn bimetallic catalysts of different atom ratios, we found that Co_6/MnO_x showed the best performance (entries 1, 9 to 11). We also tested other Co based bimetallic catalyst prepared by a similar method, including Co_6/ZnO_x, Co_6/AlO_x, and Co_6/CeO_x, but the results were poor (entries 12 to 14). Thus, Co_6/MnO_x was appropriate for the reaction.

The solvent was also important for the reaction. Without solvent, the reaction could take place at lower activity and selectivity (Table 1, entry 15). Both squalane and cyclohexane as solvent could effectively improve the catalytic performance, and selectivity in squalane was slightly higher (entries 1, 16). We also tested benzene and found that the solvent aromaticity inhibited the reaction (entry 17). When we used polar solvents, such as 1,3-Dimethyl-2-imidazolidinone (DMI) and water, both reaction activity and selectivity were much lower (entries 18, 19). Interestingly, minor methanol and ethanol were observed. In short, squalane solvent and Co_6/MnO_x catalyst were a suitable combination for the reaction.

Fig. 2*A* shows the effect of reaction temperature upon the reaction activity and selectivity. The C_{5+} products began to form

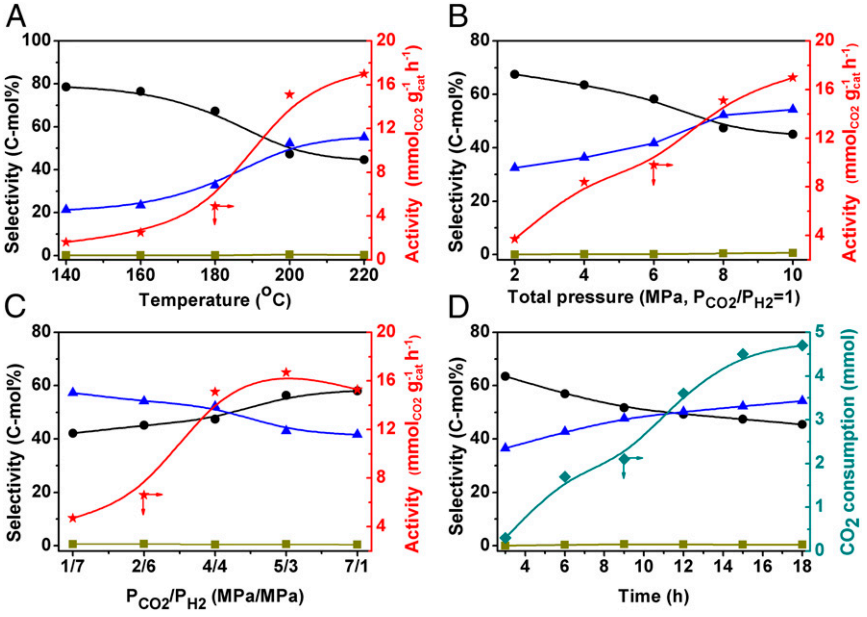

Fig. 2. Effect of reaction conditions [(*A*) reaction temperature, (*B*) total pressure, (*C*) CO_2/H_2 ratio, and (*D*) reaction time] on the CO_2 hydrogenation using 20 mg of Co_6/MnO_x and 1 mL of squalane. Other conditions: (*A*) 4 MPa of CO_2 and 4 MPa of H_2, 15 h; (*B*) P_{CO2}/P_{H2} = 1, 200 °C, 15 h; (*C*) initial pressure 8 MPa, 200 °C, 15 h; and (*D*) 4 MPa of CO_2 and 4 MPa of H_2, 200 °C. Symbols: triangle, C_{5+} selectivity; circle, C_{1-4} selectivity; square, CO selectivity; star, activity; diamond, CO_2 consumption.

at 140 °C. When the temperature was gradually elevated to 200 °C, the reaction rate and C_{5+} selectivity increased remarkably. The contribution of catalytic activity from 200 °C to 220 °C was not as significant as that from 180 °C to 200 °C. In addition, the increase of C_{5+} selectivity also became slower from 200 °C to 220 °C, suggesting that 200 °C was a suitable temperature. At this temperature, we studied the influence of the total pressure at an equal proportion of CO_2 and H_2 (Fig. 2*B*). Both the activity and C_{5+} selectivity were enhanced markedly with the elevating total pressure, while they changed slowly when the pressure exceeded 8 MPa. We further fixed the total pressure at 8 MPa and studied the influence of CO_2/H_2 ratio on the reaction (Fig. 2*C*). The activity rose rapidly with increasing CO_2 pressure, which became less evident when the ratio of CO_2/H_2 reached 4/4. On the other hand, the C_{5+} selectivity decreased with elevating CO_2 pressure, and the rate of decrease became faster after the CO_2/H_2 ratio was larger than 4/4. Thus, 4 MPa of CO_2/4 MPa of H_2 was the best for the reaction. Fig. 2*D* illustrates the time course of the reaction. The CO_2 was consumed continuously during the reaction, and the C_{5+} selectivity rose gradually with reaction time. The GC analysis also verified that the chain length of the products increased with increasing reaction time. It is noteworthy that, at all above conditions, CO was hardly detectable.

The reusability of the catalyst is shown in *SI Appendix*, Fig. S8*A*. A trend of slight decrease in selectivity and activity was observed. The TEM, N_2 adsorption, XRD, and XPS characterization also showed that the catalyst changed slightly after the recycling test (Fig. 1 and *SI Appendix*, Figs. S1, S3, and S5). In the hot filtration test, no product was generated after the catalyst was filtered out, indicating that the catalyst worked in a heterogeneous mode (*SI Appendix*, Fig. S8*B*). It should be mentioned that industrial use of a heterogeneous catalyst usually operates in a flow reactor. Further work should be done to optimize operation conditions using a flow reactor for practical application.

Reaction Mechanism. Co^0 is a well-known FTS catalyst using syngas, but it is generally regarded as a methanation catalyst in CO_2 hydrogenation (9, 16). This can be ascribed to its weak CO_2 adsorption and strong H_2 adsorption ability, which results in high H/C ratio on the catalyst surface. The high H/C ratio inhibited the chain growth process and favored methane generation (19). Inspired by this, we tested the temperature-programmed desorption of CO_2 (CO_2-TPD) of Co^0 catalyst and the Co−Mn catalysts. The results demonstrated that the amount of CO_2 adsorbed on the Co−Mn catalysts was much higher than that on Co^0 (Fig. 3*A*). In addition, CO_2 adsorption on Co_6/MnO_x was the highest in all of the catalysts, especially near the reaction temperature. The CO_2-TPD data were consistent with the catalytic results. The CO_2 desorbed at a higher temperature (e.g., 188 °C) directly correlated with the C_{5+} selectivity. The H_2 adsorption ability of the catalyst was also crucial. The H_2-TPD analysis revealed that the amount of H_2 adsorbed on Co_6/MnO_x was remarkably lower than that on the Co^0 catalyst, especially at higher temperature (150 °C to 250 °C; Fig. 3*B*). The above results verified that the C/H ratio on Co_6/MnO_x must be much higher than that on Co^0, accounting for the exceptional behavior of Co_6/MnO_x. We would like to mention that competitive adsorption of the reactant gases (e.g., CO_2, H_2) on the catalyst surface existed at reaction conditions. We further conducted the CO_2-TPD and H_2-TPD characterization of other Co-based bimetallic catalysts (Co_6/ZnO_x, Co_6/AlO_x, Co_6/CeO_x), as shown in Fig. 3 *C* and *D*. The results demonstrated that addition of Zn, Al, and Ce promoters excellently accelerated the CO_2 adsorption, but could not suppress or even promote the H_2 adsorption on the catalyst, while addition of Mn promoter to Co catalyst not only remarkably enhanced the CO_2 adsorption but also significantly suppressed the H_2 adsorption. This is the reason Mn is the appropriate promoter for producing long-chain paraffins. The TPD data could also explain why the C_{5+} selectivity over Co_6/ZnO_x was higher than those over Co_6/AlO_x and Co_6/CeO_x (Table 1, entries 12 to 14).

We characterized Co_6/MnO_x catalyst pretreated with H_2 at 200 °C by the semi-in situ XPS method. The result revealed that, at reaction condition, Co^0/Co^{2+} coexisted on the catalyst surface and Mn^{3+} was in situ reduced to Mn^{2+} (*SI Appendix*, Fig. S5 *D*–*F*). The outstanding performance of Co_6/MnO_x may be due to the synergy of the surface Co^0, Co^{2+}, and Mn^{2+} atoms during the

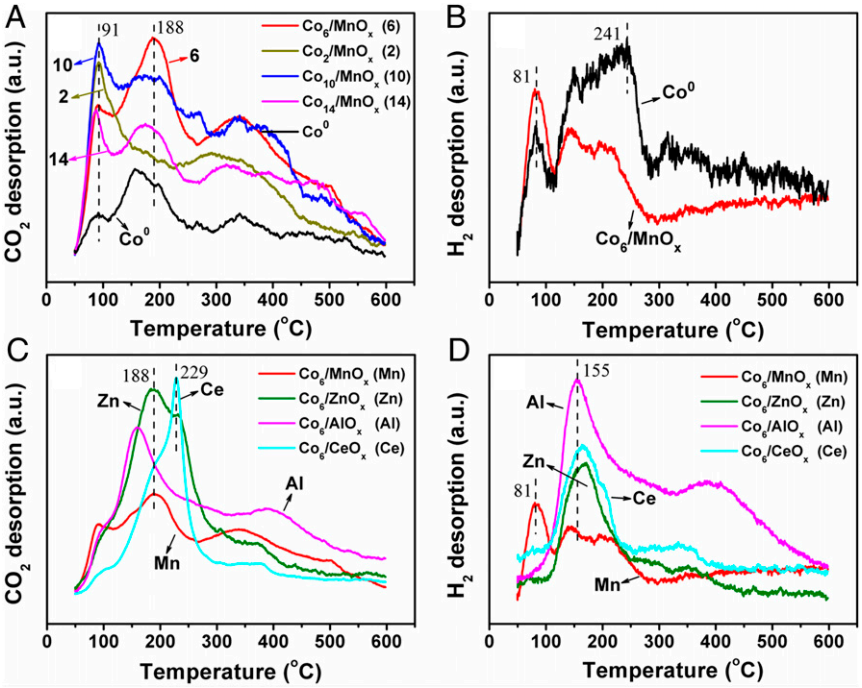

Fig. 3. CO_2-TPD (*A* and *C*) and H_2-TPD (*B* and *D*) data of the catalysts. The TPD signals have been normalized to the mass of the tested samples.

reaction. The semi-in situ XPS study also manifested that the CO_2 adsorption was improved when the temperature increased from 50 °C to 150 °C (*SI Appendix*, Fig. S9). At 200 °C, the adsorbed CO_2 was reduced to hydrocarbons by the H atoms preadsorbed on the catalyst surface. To detect the intermediates of the reaction, we further conducted an in situ Fourier transform infrared (FTIR) study of CO_2 adsorption on the pretreated catalyst at 200 °C. The result of the in situ FTIR study is shown in Fig. 4. It can be seen that CO_2 was adsorbed on the catalyst surface and gradually reduced to CH_2/CH_3, via $CO_2^{\delta-}$, $HCOO^-$, $-CH_2OH$, and/or CH_3O^- intermediates (Fig. 4*A*). The weak peak at 1,434 cm^{-1} is assigned to asymmetrically adsorbed CO_2 (CO_3^{2-}). At 2 min, it was quickly reduced to $CO_2^{\delta-}$ by H atoms on the catalyst surface, as can be seen from the peaks at 1,289 and 1,606 cm^{-1}. At 2.5 min, it was observed that formate ($HCOO^-$) species began to form by reducing $CO_2^{\delta-}$. The peaks at 1,373 and 1,594 cm^{-1} correspond to symmetric and asymmetric OCO stretches of $HCOO^-$. The $HCOO^-$ was further reduced to primary alcohol group (-CH_2OH, 1,028 cm^{-1}) and/or methoxy group (CH_3O^-, 1,068 cm^{-1}). Finally, the $-CH_2OH$/CH_3O^- were reduced to CH_2 group (1,474 cm^{-1}) and/or CH_3 group (1,388 cm^{-1}). The broad peak around 1,474 cm^{-1} revealed the coexistence of the CH_2 and CH_3 groups. No carboxylic acid, alcohol, or ether was detected in the reaction product, indicating that the $HCOO^-$, $-CH_2OH$, and/or CH_3O^- intermediates were finally converted into CH_2 and/or CH_3. With the consumption of $HCOO^-$, $-CH_2OH$, and/or CH_3O^- species, the peaks of CH_2 and CH_3 became more and more remarkable, which further proved such conversion. The peak at 843 cm^{-1} can be attributed to out-of-plane bending vibration of C–H in alkenes. The assignment of the above peaks agrees well with that in the literature (20). No gaseous CO or adsorbed CO (CO_{ad}) was observed (Fig. 4*B*). The FTIR study suggested that the reaction did not proceed through the CO pathway.

Only a very little CO was detected during the reaction over Co_6/MnO_x (Fig. 2), which agreed with the very low RWGS ability of the Co catalyst (9, 16). Moreover, addition of Mn to Co-based catalyst may accelerate the dissociation and disproportionation of CO (21). To investigate the contribution of the trace CO in the C_{5+} hydrocarbons synthesis, we conducted the reaction using CO (0.5 MPa, 4 MPa) instead of CO_2. It was observed that the reaction rate was much lower, and little C_{5+} product was observed (*SI Appendix*, Table S2, entries 1, 2). The products were mostly C_1–C_4 hydrocarbons with a small amount of methanol and ethanol, which were different from those in CO_2 hydrogenation. The CO-TPD and H_2-TPD data indicate that addition of Mn promoter inhibited the adsorption of CO and H_2 on the Co catalyst, especially at the reaction temperature (200 °C) (Fig. 3*B* and *SI Appendix*, Fig. S10). Furthermore, most of the Co atoms on the catalyst surface were blocked by the carbon deposit after the CO hydrogenation (*SI Appendix*, Fig. S11). The TEM and XPS data also suggested that CO altered the Co/Mn valence and resulted in surface reconstruction (Fig. 1 and *SI Appendix*, Fig. S5). These facts help to explain the poor result of CO hydrogenation over Co_6/MnO_x. We further conducted a ^{13}CO labeling test by adding a small amount of ^{13}CO in the reactant gases (i.e., 0.2 MPa of ^{13}CO, 3.8 MPa of CO_2, 4 MPa of H_2). The gas chromatography mass spectrometry (GC-MS) spectra of this test are shown in *SI Appendix*, Fig. S12. As expected, both ^{13}CO and CO_2 could generate the target paraffins, whereas the ^{13}C of ^{13}CO did not enter the products generated from CO_2, and the CO_2 did not take part in the products formed by ^{13}CO either. This phenomenon revealed that the CO_2 and ^{13}CO formed long-chain paraffins separately and independently in the reaction. There is a strong possibility that hydrogenation of CO_2 and CO proceeded on segregated and different sites of the catalyst. Otherwise, the $^{13}CH_2$ monomer from ^{13}CO and the CH_2 monomer from CO_2 would enter the same paraffin molecule. The surface segregation of the cobalt catalyst during the FTS reaction has been reported elsewhere (22). The results of the ^{13}CO labeling test further confirmed that hydrogenation of CO_2 to produce paraffins over Co_6/MnO_x did not proceed via CO. We also used CH_3OH or HCOOH, instead of CO_2, to react with H_2, but the results were poor (*SI Appendix*, Table S2, entries 3 and 4). This may be because the dissociative adsorption of formic acid and methanol on the catalyst surface was difficult at the reaction condition, which was necessary for further transformation.

Based on all of the results above, we proposed the possible reaction mechanism. Firstly, CO_2 and H_2 adsorbed on the Co_6/MnO_x surface, where the Mn promoter enhanced the CO_2 adsorption and weakened the H_2 adsorption. Secondly, the adsorbed CO_2 was reduced to CH_2 and CH_3 by H atoms on the catalyst, via $CO_2^{\delta-}$, $HCOO^-$, $-CH_2OH$, and/or CH_3O^- intermediates. The CH_2 is known as the principle monomer in FTS reactions, while the CH_3 species are common starters for chains to grow (22). Finally, the liquid hydrocarbons were formed by chain growth steps with CH_2 and CH_3. The largest molecule in the product had 26 C atoms, and the product distribution followed the ASF statistics ($\alpha = 0.78$), indicating that the chain growth steps are very similar to those of the well-known Co^0 catalyzed FTS reaction (22). The presence of Co^0 atoms on the Co_6/MnO_x surface at reaction condition further supported this mechanism. The major mechanistic contribution of this work is direct formation of CH_2/CH_3 in CO_2 hydrogenation, not via CO. Obviously, the parts of the pathway related to FTS are consistent with the well-established Fischer–Tropsch chemistry (e.g., the monomer, the chain growth process, and the ASF distribution of products).

Concluding Remarks

In summary, we discovered a simple Co_6/MnO_x nanocatalyst that could efficiently catalyze CO_2 hydrogenation to normal C_{5+} hydrocarbons at a lower temperature. Co was the major catalyst, while Mn promoter enhanced CO_2 adsorption and weakened H_2 adsorption on the catalyst. During the reaction, CO_2 adsorbed

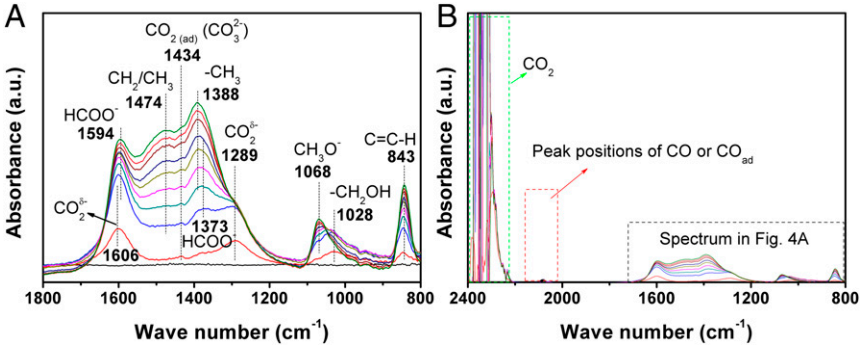

Fig. 4. In situ FTIR spectra [(*A*) key intermediates and (*B*) wide band] recorded during the CO_2 adsorption on Co_6/MnO_x. The catalyst was pretreated with H_2 at 200 °C for 2 h before the adsorption test. The black straight line at the bottom was the baseline recorded before CO_2 adsorption. The spectra were recorded after the CO_2 was introduced to the catalyst, and the time sequence, from bottom to top, was 2, 2.5, 4.5, 7.5, 15, 25, 35, 45, and 55 min.

on the catalyst and was reduced by H atoms to CH_2 monomer and CH_3 species, via $CO_2^{\delta-}$, $HCOO^-$, $-CH_2OH$, and/or CH_3O^- intermediates. The liquid hydrocarbons were generated by further chain growth steps, which are similar to those of the well-known Co^0 catalyzed FTS reaction. The reaction could proceed by avoiding CO, which opens an avenue for liquid fuel synthesis and CO_2 transformation.

Materials and Methods

Catalyst Preparation. The Co–Mn bimetallic catalysts were prepared by a coprecipitation method. In a typical procedure, $Co(NO_3)_2{\cdot}6H_2O$ (0.873 g, 3.0 mmol) and $Mn(NO_3)_2{\cdot}4H_2O$ (0.125 g, 0.5 mmol) were dissolved in 40 mL of water and were stirred for 1 h. Then the solution was added into 100 mL of Na_2CO_3 solution (0.5 mol/L) within 1 h of stirring. After stirring for another 3 h, the solid was centrifuged and washed with 500 mL of water. It was dried at 110 °C for 10 h and calcined at 400 °C for 3 h, and was reduced under hydrogen flow at 400 °C for 1 h. Finally, the catalyst was passivated with a low content of oxygen (e.g., 1%) in N_2 at room temperature for 30 min, and Co_6/MnO_x was obtained. The catalysts with Co/Mn molar ratios of 2, 10, and 14 were also prepared using a similar method. Co_6/ZnO_x, Co_6/AlO_x, and Co_6/CeO_x were also fabricated by the above method, using $Co(NO_3)_2{\cdot}6H_2O$ to react with $Zn(NO_3)_2{\cdot}6H_2O$, $Al(NO_3)_3{\cdot}9H_2O$, and $Ce(NO_3)_3{\cdot}6H_2O$, respectively. Furthermore, the metallic Co catalyst (Co^0) was synthesized by a similar method, during which $Co(NO_3)_2{\cdot}6H_2O$ (0.873 g, 3.0 mmol) was used as precursor. The source and specification of the chemicals used in this work are given in *SI Appendix*. The catalysts fabricated above had good air stability.

Catalyst Characterization. The as-prepared catalysts were characterized by N_2 adsorption, XRD, XPS, TEM, ICP-OES, H_2-TPR, and TPD. More experimental details are provided in *SI Appendix*.

In Situ Characterization. The semi-in situ XPS measurement was aided by a special vacuum seal sample unit to transfer the sample prepared in the glove box. To study the CO_2 adsorption, Co_6/MnO_x was pretreated with 4 MPa of H_2 at 200 °C for 2 h. The reactor was cooled, and the H_2 was released and replaced with 1 MPa of CO_2 three times. Then the reactor was charged with 2 MPa of CO_2 and kept at the specified temperature for 1 h. Finally, the reactor was cooled to room temperature, and the gases were released. The sample was prepared in a glove box, and transferred to the sample chamber of an XPS spectrometer using the sample unit. To reduce the loss of adsorbates during the XPS analysis, the sample chamber was kept at ultra-low temperature using liquid nitrogen.

The in situ FTIR spectra were recorded with a Nicolet FTIR Spectrometer 6700 equipped with a liquid-nitrogen-cooled narrow-band mercury–cadmium–telluride detector and diffuse reflectance infrared Fourier transform spectroscopy optics. The details of the apparatus and operation procedure were described elsewhere (23). To get clear spectra, the black Co_6/MnO_x and KBr powders were mixed and ground together. Then the mixture was pressed into the sample cup. At 200 °C, the sample was firstly purged with N_2 for 2 h, then it was treated with H_2 for 2 h. After further purging the sample with N_2 for 1 h, CO_2 was introduced to the sample, and the CO_2 adsorption began. All of the above experiments were conducted at ambient pressure. The flow rate of the above gases was 200 mL/min. A background spectrum was recorded before CO_2 adsorption. Spectra were collected as difference spectra with the background spectrum. The surface products were shown as positive bands, while loss of surface species was shown as negative bands. In this way, the formation and disappearance of the surface species during the process can be clearly recorded.

CO_2 Hydrogenation. The CO_2 hydrogenation was conducted in a 16-mL stainless steel batch reactor with a Teflon lining. In a typical experiment, the catalyst (20 mg) and solvent (1.0 mL) were added in the reactor under air. The reactor was sealed, and the air was removed by flushing with 1 MPa of CO_2 three times. Then, 4 MPa of CO_2 and 4 MPa of H_2 were charged at room temperature. The reaction was performed at 200 °C for the desired time. Then the reactor was cooled in an ice-water bath, and the gas was released slowly and collected for analysis in an HP 4890B GC with thermal conductivity detector. The liquid products were analyzed in an HP 7890B GC with flame ionization detector using toluene as an internal standard. The liquid products were identified using GC-MS (Agilent-7890B-5977A) as well as by comparing the retention times with the standards in the GC traces. The yields of the products were calculated from the GC data. The conversion of CO_2 was calculated from the amount of reacted CO_2 divided by the total CO_2 added to the reactor. The total amount of CO_2 charged into the reactor could be obtained by weighing, and the reacted CO_2 was known from the amount of total carbon in the product.

The Recycling Test. The solid catalyst was separated and washed with cyclohexane (5 × 3 mL) and dried under vacuum at 60 °C for 10 h. Then the catalyst was used directly for the next run.

The Hot Filtration Test. The hot filtration test was conducted at typical reaction conditions. After 6 h, the catalyst was filtered, and the solution was analyzed by GC. The reaction in the resulting solution proceeded for another 9 h, and then the reaction solution was analyzed again by GC.

ACKNOWLEDGMENTS. We thank Shengrui Tong and Kaihui Xia for the in situ FTIR test; Zhijuan Zhao, Xiaoyu Zhang, and Baolong Qu for XPS analysis; and Yang Sun and Xiang Hao for XRD characterization. This work is supported by the National Natural Science Foundation of China (Grants 21875262, 21533011, 21733011, and 21706152), National Key Research and Development Program of China (Grant 2017YFA0403102), Beijing Municipal Science & Technology Commission (Grant Z181100004218004), and the Chinese Academy of Sciences (Grant QYZDY-SSW-SLH013).

1. M. He, Y. Sun, B. Han, Green carbon science: Scientific basis for integrating carbon resource processing, utilization, and recycling. *Angew. Chem. Int. Ed. Engl.* **52**, 9620–9633 (2013).
2. M. Aresta, *Carbon Dioxide as Chemical Feedstock* (Wiley-VCH, Weinheim, 2010).
3. Q. Liu, L. Wu, R. Jackstell, M. Beller, Using carbon dioxide as a building block in organic synthesis. *Nat. Commun.* **6**, 5933 (2015).
4. J. Graciani *et al*., Catalysis. Highly active copper-ceria and copper-ceria-titania catalysts for methanol synthesis from CO_2. *Science* **345**, 546–550 (2014).
5. Q. Qian, J. Zhang, M. Cui, B. Han, Synthesis of acetic acid via methanol hydrocarboxylation with CO_2 and H_2. *Nat. Commun.* **7**, 11481 (2016).
6. X. B. Li, C. H. Tung, L. Z. Wu, Semiconducting quantum dots for artificial photosynthesis. *Nat. Rev. Chem.* **2**, 160–173 (2018).
7. M. H. Cano, K. Agbossou, S. Kelouwani, Y. Dube, Experimental evaluation of a power management system for a hybrid renewable energy system with hydrogen production. *Renew. Energy* **113**, 1086–1098 (2017).
8. W. Wang, S. Wang, X. Ma, J. Gong, Recent advances in catalytic hydrogenation of carbon dioxide. *Chem. Soc. Rev.* **40**, 3703–3727 (2011).
9. G. Prieto, Carbon dioxide hydrogenation into higher hydrocarbons and oxygenates: Thermodynamic and kinetic bounds and progress with heterogeneous and homogeneous catalysis. *ChemSusChem* **10**, 1056–1070 (2017).
10. J. Klankermayer, S. Wesselbaum, K. Beydoun, W. Leitner, Selective catalytic synthesis using the combination of carbon dioxide and hydrogen: Catalytic chess at the interface of energy and chemistry. *Angew. Chem. Int. Ed. Engl.* **55**, 7296–7343 (2016).
11. A. Álvarez *et al*., Challenges in the greener production of formates/formic acid, methanol, and DME by heterogeneously catalyzed CO_2 hydrogenation processes. *Chem. Rev.* **117**, 9804–9838 (2017).
12. P. G. Jessop, F. Joó, C. C. Tai, Recent advances in the homogeneous hydrogenation of carbon dioxide. *Coord. Chem. Rev.* **248**, 2425–2442 (2004).
13. Z. H. He *et al*., Water-enhanced synthesis of higher alcohols from CO_2 hydrogenation over a Pt/Co_3O_4 catalyst under milder conditions. *Angew. Chem. Int. Ed.* **55**, 737–741 (2016).
14. J. Wei *et al*., Directly converting CO_2 into a gasoline fuel. *Nat. Commun.* **8**, 15174 (2017).
15. P. Gao *et al*., Direct conversion of CO_2 into liquid fuels with high selectivity over a bifunctional catalyst. *Nat. Chem.* **9**, 1019–1024 (2017).
16. R. W. Dorner, D. R. Hardy, F. W. Williams, H. D. Willauer, Heterogeneous catalytic CO_2 conversion to value-added hydrocarbons. *Energy Environ. Sci.* **3**, 884–890 (2010).
17. Y. H. Choi *et al*., Carbon dioxide Fischer-Tropsch synthesis: A new path to carbon-neutral fuels. *Appl. Catal. B* **202**, 605–610 (2017).
18. G. E. Batley, A. Ekstrom, D. A. Johnson, Studies of topochemical heterogeneous catalysis: 3. Catalysis of the reduction of metal oxides by hydrogen. *J. Catal.* **34**, 368–375 (1974).
19. C. G. Visconti *et al*., Fischer–Tropsch synthesis on a Co/Al2O3 catalyst with CO2 containing syngas. *Appl. Catal. A* **355**, 61–68 (2009).
20. L. Wang *et al*., Selective hydrogenation of CO_2 to ethanol over cobalt catalysts. *Angew. Chem. Int. Ed. Engl.* **57**, 6104–6108 (2018).
21. Z. Zhao *et al*., Insight into the formation of $Co@Co_2C$ catalysts for direct synthesis of higher alcohols and olefins from syngas. *ACS Catal.* **8**, 228–241 (2018).
22. H. Schulz, Major and minor reactions in Fischer–Tropsch synthesis on cobalt catalysts. *Top. Catal.* **26**, 73–85 (2003).
23. S. R. Tong, L. Y. Wu, M. F. Ge, W. G. Wang, Z. F. Pu, Heterogeneous chemistry of monocarboxylic acids on α-Al_2O_3 at different relative humidities. *Atmos. Chem. Phys.* **10**, 7561–7574 (2010).